Single-chain magnet behavior in a 2p–3d–4f spin array with a nitronyl nitroxide biradical

Juan Sun, Jing Xie, Licun Li, Jean-Pascal Sutter

Single-chain magnet behavior in 2p-3d-4f spin array with nitronyl nitroxide biradical

Juan Sun,[a] Jing Xie,[a] Licun Li,*[,a] Jean-Pascal Sutter*[,b]

[a] *Department of Chemistry, Key Laboratory of Advanced Energy Materials Chemistry, College of Chemistry, Nankai University, Tianjin 300071, China*
E-mail: llicun@nankai.edu.cn

[b] *Laboratoire de Chimie de Coordination du CNRS (LCC-CNRS) Université de Toulouse, CNRS, Toulouse, France*
E-mail: sutter@lcc-toulouse.fr

Abstract

Three biradical-bridged heterometallic chains, $[LnCu_2(hfac)_7(bisNITPhPy)]_n$ (Ln^{III} = Gd, **1**; Tb, **2**; Ho, **3**), were synthesized by means of nitronyl nitroxide biradical bisNITPhPy ([5-(4-pyridyl)-1,3-bis(1′-oxyl-3′-oxide-4′,4′,5′,5′-tetramethyl-4,5-hydro-1*H*-imidazol-2-yl)]benzene; hfac = hexafluoroacetylacetonate). In these structures, the bisNITPhPy biradical serves as a pentadentate ligand to hold one Ln^{III} ion through two neighboring aminoxyl (NO) moieties in chelating mode, while other two NO groups are coordinated to $Cu(hfac)_2$ units, leading to a 1D Cu-Ln-birad chain. An additional terminal $Cu(hfac)_2$ unit linked to pyridine-N atom is found at the periphery. The magnetic susceptibility data of compound Gd have been analyzed with a closed ring model comprising three [Cu-Rad-Gd-Rad] units, which indicate the ferromagnetic Gd(III)-nitroxide and Cu(II)-axial nitroxide interactions. Tb derivative was found to behave as a single chain magnet with an energy barrier for magnetization reversal of 26 K.

Introduction

Single molecule magnets (SMMs) and single chain magnets (SCMs) are discrete and 1-D molecular compounds that are characterized by a slow relaxation of their magnetizations below a critical temperature. Such species have attracted increasing attention due to application prospects in information storage, and quantum computing, etc.[1] This triggered in recent years tremendous work dedicated to SMMs,[2] in contrast, the investigations addressing to SCMs remain rather limited.

SCM behavior was predicted in 1963 by Glauber,[3] yet the first SCM, a radical-bridged Co(II) chain was achieved only four decades later by Gatteschi et al.[4] In this 1D coordination polymer Co(II) centers are associated to nitronyl nitroxide radicals (NIT hereafter) acting as bridging ligands. To possess a SCM behavior the molecular system must satisfy three key parameters: (i) its magnetic anisotropy must be uni-axial and large, (ii) efficient exchange interactions should take place between the magnetic centers, and (iii) the individual chains must be magnetically shielded from each other.[5] It is, however, still a great challenge to assemble SCMs, and one difficulty resides in achieving strong intra-chain magnetic interactions to reach large correlation energies and minimize the effect of intermolecular interactions. In this respect the metal-nitronyl nitroxide radical approach is an efficient and exciting strategy for constructing SCMs,[4,6,7] where the nitronyl nitroxide radicals serve as bridging ligands ensuring for strong magnetic interactions. This approach yielded some examples of SCMs when anisotropic ions(ex. Co(II) or Ln(III) ions) were involved.[4,6,7] Recently, SCM behavior was also reported for heterotrispin Cu-Ln-nitronyl nitroxide radical chains.[8]

The large magnetic anisotropy of Ln(III) ions such as Tb(III) or Dy(III) makes them appealing building units to construct SCMs.[9] However, despite a reasonable ferromagnetic interaction with aminoxyl radical,[10] the resulting energy barriers for magnetization flipping of the 1D array remain modest. A likely origin for this is the next-neighbor antiferromagnetic radical-radical interactions mediated by the Ln center that compete with the Ln-Radical ferromagnetic interactions. Recently, we disclosed an example suggesting that a ferromagnetic diradical ligand could allow reducing the effect of the next-neighbor contribution. The biradical-bridged Cu^{II}-Dy^{III} chain with formula $[DyCu_2(hfac)_7(bisNITPhPy)]_n$ (bisNITPhPy stands for [5-(4-pyridyl)-1,3-bis(1′-oxyl-3′-oxide-4′,4′,5′,5′-tetramethyl-4,5-hydro-1*H*-imidazol-2-yl)]benzene, Scheme 1),[11] was found to exhibit SCM behavior with increased energy barrier for spin-flip as compared to a mono-radical homologue. As an extension of that study, we examined the effect of alternating the Ln ion and report herein three related bisNITPhPy-Cu^{II}-Ln^{III} chains made up with Gd (**1**), Tb (**2**), and Ho (**3**). Remarkably, the Tb derivative was found to behave as a SCM and the Ho homologue exhibited the

onset of slow relaxation of its magnetization just above 2 K.

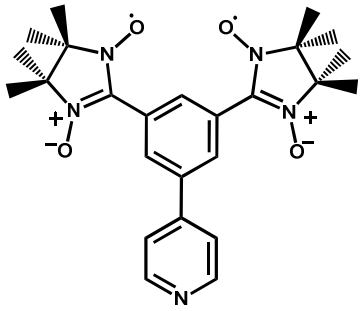

Scheme 1. bisNITPhPy biradical ligand.

Experimental section

Materials and Methods

The bisNITPhPy biradical was obtained following the literature methods.[12] Purchased chemicals for synthesis were used as-received. IR data were measured on a Bruker Tensor 27 Spectrophotometer using pressed KBr pellets. Elemental analyses were performed using a Perkin-Elmer 240 elemental analyzer. Powder X-ray diffraction (PXRD) data were recorded using a Rigaku Ultima IV diffractometer. Magnetic measurements were carried out on Quantum Design MPMS 5 SQUID and PPMS-9 magnetometers using polycrystalline samples embedded in grease. Magnetic susceptibility between 2 and 300 K was collected in a field of 1 kOe. AC susceptibility responses have been collected in the frequency range 10 – 10^4 Hz with an AC field of 3 Oe. Diamagnetic corrections for the magnetic susceptibility data have been made based on Pascal's constants[13] and the sample holder contribution.

Synthesis of $[LnCu_2(hfac)_7(bisNITPhPy)]_n$ (Ln = Gd, **1**; Tb, **2**; Ho, **3**)

A mixture of $Ln(hfac)_3{\cdot}2H_2O$ (0.01 mmol) and $Cu(hfac)_2$ (0.02 mmol, 0.0096 g) was dissolved in 15 mL dry boiling *n*-hexane and the resulted solution was refluxed for 6 h. Then the mixture was cooled to 50 °C and a $CHCl_3$ solution (6 ml) of bisNITPhPy radical (0.01 mmol, 0.0047 g) was added. The final reaction was heated for 30 min under stirring. After cooling, the dark-green filtrate was allowed to stand at room temperature and slowly evaporated. After two days, dark-green strip crystals were obtained.

For **1**, yield: 65%. Elem. Anal. found (calcd) for $C_{60}H_{38}Cu_2F_{42}GdN_5O_{18}$ (%): C, 32.76 (32.77), H, 1.71 (1.74), N, 3.20 (3.18). IR(KBr): 3420(w), 2874(m), 2458(m), 1795(s), 1652(s), 1537(s), 1468(s), 1358(s), 1160(s), 1071(s), 952(s), 854(s), 661(s), 588(m), 545(s) cm^{-1}.

For **2**, yield: 52%. Elem. Anal. found (calcd) for $C_{60}H_{38}Cu_2F_{42}TbN_5O_{18}$ (%):C, 32.62 (32.74), H, 1.84 (1.74), N, 2.99 (3.18). IR(KBr): 3420(w), 2878(m), 2455(m), 1801(s), 1656(s), 1537(s), 1462(s), 1358(s), 1160(s), 1071(s), 952(s), 854(s), 661(s),

588(m), 545(s) cm^{-1}.

For **3**, yield: 62%. Elem. Anal. found (calcd) for $C_{60}H_{38}Cu_2F_{42}HoN_5O_{18}$ (%): C, 32.51 (32.65), H, 1.80 (1.74), N, 3.16 (3.17). IR(KBr): 3416(s), 2872(m), 2457(m), 1791(m), 1648(s), 1533(s), 1477(s), 1357(s), 1156(s), 1074(s), 948(s), 856(s), 662(s), 588(m), 545(s) cm^{-1}.

X-ray structure determination

Single crystal X-ray diffraction analyses were implemented on a Rigaku Saturn CCD diffractometer (Mo Kα radiation, λ = 0.71073 Å) for **1** and **2** at 113 K and a Rigaku 007HF XtaLAB P200 diffractometer (Cu Kα radiation, λ = 1.54178 Å) for **3** at 120 K. Multiscan absorption corrections were carried out using the SADABS program. The programs SHELXS-2014 and SHELXL-2014 were used to solve and refine the structures by direct methods and full-matrix least-squares based on F^2.[14] All non-hydrogen atoms were refined anisotropically and the hydrogen atoms of bisNITPhPy radical and $hfac^-$ ligands were placed in calculated positions and refined using a riding model. To rationalize the disorder CH_3/CF_3 groups, the restraints of DFIX, ISOR, SIMU, and DELU were applied. Crystal data and structure refinements for **1**-**3** are provided in Table 1. Key bond lengths/angles of **1**-**3** are listed in Tables 2 and S1-S3. CCDC numbers for **1**, **2** and **3** are 1978786-1978788, respectively.

Table 1.Crystallographic data for **1**-**3**.

Complexes	**1**	**2**	**3**
Empirical formula	$C_{60}H_{38}Cu_2F_{42}GdN_5O18$	$C_{60}H_{38}Cu_2F_{42}TbN_5O_{18}$	$C_{60}H_{38}Cu_2F_{42}HoN_5O_{18}$
Mr	2199.28	2200.95	2206.98
T (K)	113	113	120
Crystal system	monoclinic	monoclinic	monoclinic
Space group	$P2_1/c$	$P2_1/c$	$P2_1/c$
a/Å	21.017(4)	21.025(4)	20.8049(2)
b/Å	20.553(4)	20.566(4)	20.4248(2)
c/Å	19.031(4)	19.032(4)	18.9509(2)
β/°	95.21(3)	95.42(3)	95.6030(1)
V/$Å^3$	8187(3)	8193(3)	8014.4(4)
Z	4	4	4
D_{calcd}/g cm^{-3}	1.784	1.784	1.829
μ/mm^{-1}	1.476	1.529	3.909
θ/°	1.462 to 25.009	2.150 to 25.010	3.709 to 74.450
F(000)	4308	4312	4319

Collected reflections	77893	76407	48917
Independent reflections	14431	14232	15872
R_{int}	0.0690	0.0807	0.0310
GOF(F^2)	1.085	1.105	1.070
R_1/wR_2 [I > 2σ(I)][a]	0.0783/0.2113	0.0923/0.2375	0.0848/0.2436
R_1/wR_2 (all data)[a]	0.0989/ 0.2322	0.1175/0.2581	0.0919/0.2516

[a] $R_1 = \Sigma(||Fo| - |Fc||)/\Sigma|Fo|$, $wR_2 = [\Sigma w(|Fo|^2 - |Fc|^2)^2/\Sigma w(|Fo|^2)^2]^{1/2}$

Table 2. Key bond lengths/angles [Å/°] for **1**-**3**.

	1	**2**	**3**
Ln-O(rad)	2.386(5), 2.393(5)	2.383(6), 2.391(6)	2.359(4), 2.362(4)
Ln-O(hfac)	2.318(5)-2.385(5)	2.312(6)-2.384(7)	2.284(4)-2.366(4)
Ln-O-N	136.8(5), 139.2(4)	137.9(6), 139.3(5)	136.6(4), 138.7(3)
Cu1-N	2.033(7)	2.031(8)	2.025(5)
Cu2-O(rad)	2.386(6)	2.383(7)	2.372(4)
Cu2-O(hfac)	1.927(6), 1.934(6)	1.927(6), 1.923(8)	1.940(4), 1.934(5)
Cu2-O-N	149.2(6)	150.1(8)	147.3(5)
Cu3-O(rad)	2.611(6)	2.610(7)	2.583(4)
Cu3-O(hfac)	1.936(6), 1.927(5)	1.941(6), 1.922(6)	1.930(4), 1.940(4)
Cu3-O-N	144.3(5)	145.0(6)	143.8(4)

Results and discussion

The compounds **1**-**3** have been prepared in a one-pot procedure using stoichiometric ratio for the reagents. They have being isolated as crystalline solids with reasonable yields (50-65 %). These crystals were suitable for structure investigation (see below) and their phase purity was confirmed by PXRD (Fig. S1).

Description of the Crystal Structures

Complexes **1-3** are isomorphous and crystallize in the $P2_1/c$ space group (Table 1). They consist in 1D coordination polymers made of Ln(III) and Cu(III) interlinked by the bisNITPhPy ligand, and exhibit a structure identical to that of the Dy^{III} analogue.[11] The structure of the Tb derivative **2** is shortly described below as a representative.

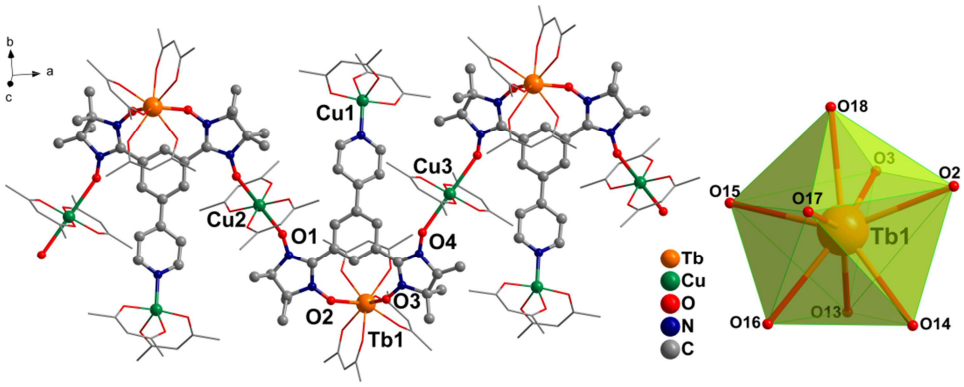

Fig. 1. One-dimensional structure of compound 2 and coordination polyhedron of Tb(III) ion (H and F atoms are omitted).

The asymmetric unit of **2** comprises one $Tb(hfac)_3$ unit, one full (Cu1) and two half (Cu2 and Cu3) $Cu(hfac)_2$ moieties, and one bisNITPhPy biradical. The bisNITPhPy ligand binds one $Tb(hfac)_3$ in chelating mode through two neighboring aminoxyl groups (Tb-O_{rad}: 2.383(6) and 2.391(6) Å), while two other NO units are coordinated to Cu2 and Cu3 ions. Each of these Cu centers is further connected to a NIT moiety of another ligand thus developing a 1D array with [-Cu-NIT-Tb-NIT-] sequence. This chain is decorated by additional $Cu(hfac)_2$ moieties linked to the pyridine-N atoms of the bisNITPhPy ligands. The coordination sphere of Tb(III) is completed by six O atoms from three bidentate $hfac^-$ ligands (Tb-O_{hfac}: 2.312(6)-2.384(7) Å). SHAPE analysis[15] suggests an almost biaugmented trigonal prism (C_{2v}) coordination geometry for the Tb center (Table S4). Both Cu2 and Cu3 centers show an octahedral ligation environment with equatorial positions occupied by the O atoms from two $hfac^-$ coligands (Cu2-O_{hfac}: 1.927(6) and 1.923(8) Å; Cu3-O_{hfac}: 1.941(6) and 1.922(6) Å), whereas apical positions accommodate two O-bound NO units from two NIT moieties (Cu2-O_{rad}: 2.383(7) Å; Cu3-O_{rad}: 2.610(7) Å). The coordination sphere for Cu1 exhibits a distorted square pyramidal geometry with two $hfac^-$ ligands and one N atom of the bisNITPhPy ligand. The intra-chain Tb1···Cu2 and Tb1···Cu3 distances through the NIT units are 8.647 Å and 8.507 Å, respectively. Packing arrangements of compound **2** (Fig. S5) show the nearest interchain Tb···Tb and Tb···Cu separations are 10.028 Å and 10.350 Å, respectively.

Magnetic Properties

The temperature dependences of the magnetic susceptibility, χ_M, given for a $LnCu_2$bisNITPhPy unit for compounds **1**-**3**, are depicted as $\chi_M T = f(T)$ in Figure 2. The experimental $\chi_M T$ values found at 300 K are 9.63 cm^3Kmol^{-1} for **1**, 13.87 cm^3Kmol^{-1} for **2** and 16.0 cm^3Kmol^{-1} for **3**, in good agreement with the anticipated contributions of one Ln^{III} ion, and four $S = 1/2$ spins with $g = 2.0$ in the absence of exchange interactions (i.e. 9.38 cm^3Kmol^{-1} for **1**, 13.32 cm^3Kmol^{-1} for **2** and 15.57

$cm^3K\ mol^{-1}$ for **3**).

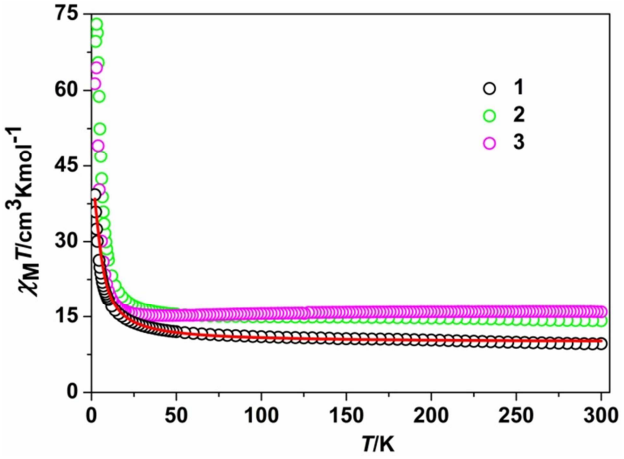

Fig. 2. Temperature-dependent $\chi_M T$ products at 1 kOe for **1-3**. The red solid line represents the calculated behavior using Magpack software for **1**(see text).

On cooling, the $\chi_M T$ values for **1** and **2** increase smoothly before increasing sharply below 50 K to reach respectively 39.29 cm^3Kmol^{-1} and 69.62 cm^3Kmol^{-1} at 2 K. For **3**, the value of $\chi_M T$ slightly decreases as T is lowered to reach 15.2 $cm^3mol^{-1}K$ for 45 K, after which a quick increase is observed with a maximum of 64.4 cm^3Kmol^{-1} at 3 K. Data recorded in a weaker field (50 Oe) for **3** do no longer exhibit the down-turn of $\chi_M T$ at low T (Figure S9, Supporting information) which indicates an effect of saturation rather than of antiferromagnetic interchain interactions. The overall variations of $\chi_M T$ *vs* T for **1**-**3** are characteristic for magnetic chains. The slight decrease for $\chi_M T$ above 50 K found in **3** is due to a marked crystal field effect for Ho(III) that leads to a significant drop of the intrinsic contribution of this ion as T diminishes.[16]

For the Gd derivative, there is no the orbital angular momentum contribution, thus the variation of $\chi_M T$ is only due to exchange interactions. A tentative insight into the strength of the magnetic couplings between spins was obtained from the simulation of the magnetic susceptibility using a closed ring model. It considered three [Cu-Rad-Gd-Rad] units (Scheme 2) with the exchange pathways J_1(Cu-radical), J_2(Gd-radical) and J_3(radical-radical), plus three independent Cu(II) ions. The spin Hamiltonian is given in Eq. 1. Simulations have been performed with the MAGPACK software.[17]

$$\hat{H} = -2J_1\left(\hat{S}_{Cu1}\hat{S}_{Rad1} + \hat{S}_{Cu2}\hat{S}_{Rad2} + \hat{S}_{Cu2}\hat{S}_{Rad3} + \hat{S}_{Cu3}\hat{S}_{Rad4} + \hat{S}_{Cu3}\hat{S}_{Rad5} + \hat{S}_{Cu1}\hat{S}_{Rad6}\right)$$
$$-2J_2\left(\hat{S}_{Gd1}\hat{S}_{Rad1} + \hat{S}_{Gd1}\hat{S}_{Rad2} + \hat{S}_{Gd2}\hat{S}_{Rad3} + \hat{S}_{Gd2}\hat{S}_{Rad4} + \hat{S}_{Gd3}\hat{S}_{Rad5} + \hat{S}_{Gd3}\hat{S}_{Rad6}\right)$$
$$-2J_3\left(\hat{S}_{Rad1}\hat{S}_{Rad2} + \hat{S}_{Rad3}\hat{S}_{Rad4} + \hat{S}_{Rad5}\hat{S}_{Rad6}\right) \qquad \text{(Eq.1)}$$

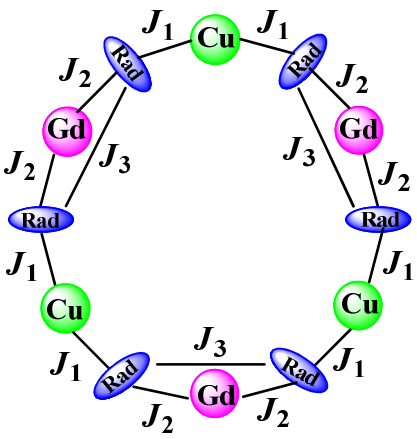

Scheme 2 Magnetic exchange pathways based on a closed ring model in compound **1**.

A good agreement between calculated and experimental data was obtained, generating the magnetic parameters J_1 = 18.56 cm^{-1}, J_2 = 3.12 cm^{-1}, J_3 = -3.10 cm^{-1} and g = 2.05. The obtained J_2 value confirms the ferromagnetic Gd(III) -nitroxide interaction**,** which is usually reported in related Gd-NIT complexes.[18] The ferromagnetic Cu-axial nitroxide interaction(J_2) can be attributed to the orthogonal magnetic orbitals of the π* SOMO (nitroxide unit) and the $d_{x^2-y^2}$ (Cu^{II} ion) orbitals).[19] J_3 reflects the overall behavior due to the NIT-NIT interaction via *m*-phenylene ring and the next-neighbor NIT-NIT interaction through the Gd^{III} ion. The former is anticipated to be ferromagnetic,[20] while latter is known to be antiferromagnetic and usually stronger than the $|J_{Gd\text{-}NIT}|$ exchange coupling.[18d,21]. The small but negative value found for J_3 suggests still a dominant next-neighbor contribution but its overall effect is much reduced in compound **1**.[22]

Dominant ferromagnetic interactions between the magnetic centers is also supported by the the isothermal *M vs H* behaviors (Fig. S7-S9). They are characterized by a fast increase of the magnetization for weak field (< 0.5 T) followed by a much smoother increase for larger fields. For Gd derivative **1**, a magnetization of 11.44 Nβ was observed for 7 T at 2 K, in agreement with the expected magnetization at saturation of 11 Nβ. For **1**, the experimental $M(H)$ curve runs above the magnetization calculated by the Brillouin equation for the independent centers (one $S = {}^7/_2$ and four $S = {}^1/_2$ with g = 2) before merging for high fields (Fig. S7), which indicates that the ferromagnetic interactions dominate the chain behavior. Furthermore, $M(H)$ curve computed using the exchange parameters deduced from $\chi_M T$ behavior matches well with experimental curve (Fig.S7), thus confirming the found parameter set.

For a chain of anisotropic spins, the $\chi_M T$ value is expected to increase exponentially at low T according to the $\chi_M T = C_{eff}\exp[\Delta_\xi/(k_B T)]$ (where C_{eff} is the effective Curie constant, Δ_ξ is the energy required to create a domain wall).[23] For Tb and Ho derivatives, a fit of the linear variation of $\ln(\chi_M T) = f(T^{-1})$ curve (Fig. 3 and S9)

yielded a correlation energy of $\Delta_\xi/k_B = 6.9$ K for **2** and 7.0 K for **3**, and respectively, C_{eff} = 13.2 and 9.3 cm^3Kmol^{-1}, thus verifying the 1D Ising-like character of these chain compounds.

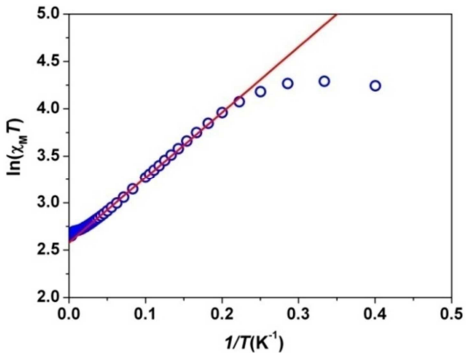

Fig. 3 $\ln(\chi_M T)$ *vs* T^{-1} plot of **2** (the solid red line represents the linear fit).

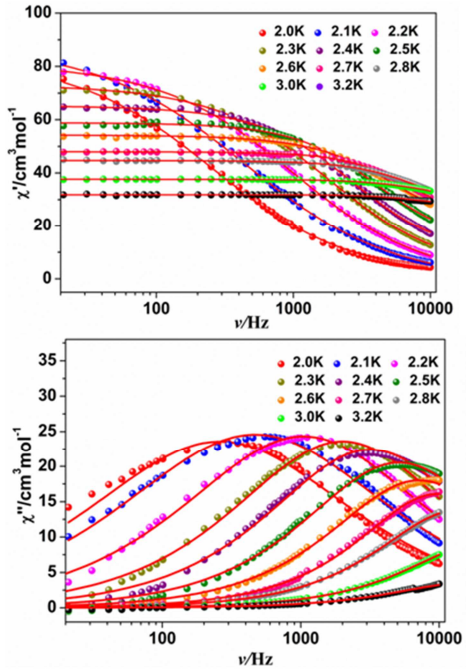

Fig. 4 Frequency-dependent ac signals under a zero dc field for compound **2** and solid lines are the fits to the Debye model.

Possible slow relaxation of the magnetization for **2** and **3** has been assessed by AC susceptibility studies in zero field; related investigations for Gd derivative **1** confirmed the absence of magnetic ordering (Fig S10). For **3** (Ho), only the onset of an out-of-phase (χ_M'') component of the magnetic susceptibility was observed below 3 K (test frequency was 1 kHz, see Fig.S12) whereas frequency and temperature dependence of peaks of in-phase (χ_M') and out-of-phase susceptibility components were observed for **2** (Fig. 4 and S11). The related Cole-Cole curves (χ_M'' *vs* χ_M', Fig.

5) display the expected semicircular shape. For **2** analysis of the frequency-dependent ac data for different temperatures with a Debye model[24] gave access to associated relaxation times τ, with distribution width (α) between 0.07 for 2.0 K and 0.38 for 3.2 K. The resulting linear variation of $\ln\tau$ *vs* T^{-1} was analyzed with the Arrhenius law $\tau = \tau_0 \exp(\Delta_\tau/k_BT)$, giving an energy barrier Δ_τ/k_B= 26.5 K with τ_0 = 8.4×10^{-10} s. This energy barrier comprises the contribution of the correlation energy, Δ_ξ, and of the blocking energy, Δ_A, due to the magnetic anisotropy of the repeating magnetic unit. Supposing the behavior of **2** is governed by a finite size regime, the anisotropy barrier can be estimated to$\Delta_A = \Delta_\tau - \Delta_\xi$ = 19.6 K.[7b]

The value of Δ_τ for **2** is somewhat lower than the one found for the homologuous Dy derivative(i.e. 40 K), but larger than the one of the SCM $[Tb_3Cu(hfac)_{11}(NitPhOPr)_4]$(*i.e.* 21 K) involving mono-nitronyl nitroxide radicals.[8a] The improvement of magnetic properties of **2** is most likely caused by much-reduced effect of the antiferromagnetic interaction between the NIT via Tb ion.

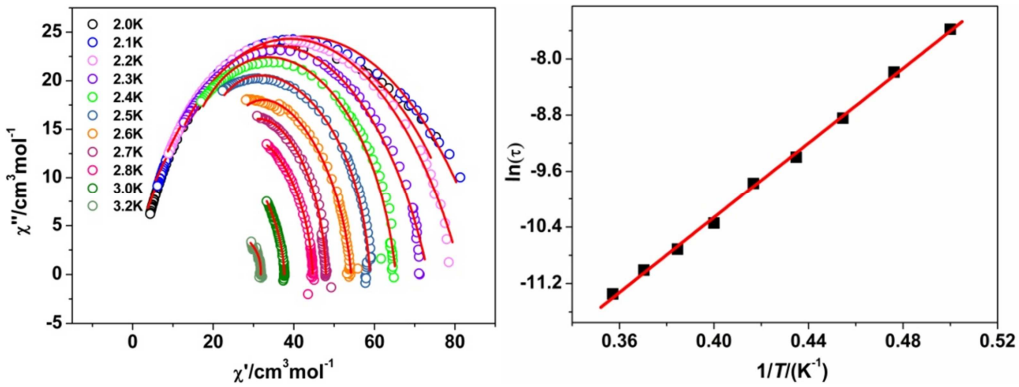

Fig. 5 (left) Cole–Cole plots of **2**. (right) $\ln\tau$ *versus* $1/T$ plot for complex **2**. The solid lines are the fitting result.

Conclusions

The results gathered herein provide further support to the potential of involving ferromagnetic biradical as bridging ligands for the construction of metal ions and aminoxyl radicals molecular magnets. It is interesting to note that for this isostructural series, slow relaxation of the magnetization was found for all the investigated Ln ions displaying magnetic anisotropy (i.e. Tb^{III}, Dy^{III}, and Ho^{III}) but the resulting SCM characteristics depend on the Ln centers. The improvement of the SCM properties of **2** compared to related 2p-3d-Tb chains may be attributed to the ferromagnetic intramolecular radical-radical interaction that should limit the destructive effect of the antiferromagnetic next-neighbor interactions. Such result highlights the utility of biradicals in developing SCMs with appealing magnetic properties.

Supporting Information

Electronic supplementary information (ESI) available: Key bond lengths and angles, SHAPE analysis for the Ln geometry, crystal structure, packing diagram, PXRD patterns, additional magnetic figures. CCDC 1978786-1978788. For ESI and crystallographic data in CIF or other electronic format see DOI:

Conflicts of interest

The authors declare no competing financial interest.

Acknowledgements

This work was financially supported by the National Key R&D Program of China (2018YFA0306002), the National Natural Science Foundation of China (No. 21773122 and 21471083) and the 111 Project (B12015).

References

1 (a) M. Affronte, Molecular nanomagnets for information technologies, *J. Mater. Chem*., 2009, **19**, 1731-1737; (b) F. Troiani and M. Affronte, Molecular spins for quantum information technologies, *Chem. Soc. Rev*., 2011, **40**, 3119-3129; (c) M. Affronte, F. Troiani, A. Ghirri, A. Candini, M. Evangelisti, V. Corradini, S. Carretta, P. Santini, G. Amoretti, F. Tuna, G. Timco and R. E. P. Winpenny, Single molecule magnets for quantum computation, *J. Phys. D: Appl. Phys*., 2007, **40**, 2999–3004; (d) M. S. Fataftah, J. M. Zadrozny, S. C. Coste, M. J. Graham, D. M. Rogers and D. E. Freedman, Employing forbidden transitions as qubits in a nuclear spin-free chromium complex, *J. Am. Chem. Soc*., 2016, **138**, 1344–1348; (e) R. Sessoli, Toward the quantum computer: magnetic molecules back in the race, *ACS Cent. Sci*., 2015, **1**, 473–474; (f) M. N. Leuenberger and D. Loss, Quantum computing in molecular magnets, *Nature*, 2001, **410**, 789-793; (g) P. C. Stamp and A. Gaita-Arino, Spin-based quantum computers made by chemistry: hows and whys, *J. Mater. Chem*., 2009, **19**, 1718-1730; (h) M. Atzori, E. Morra, L. Tesi, A. Albino, M. Chiesa, L. Sorace and R. Sessoli, Quantum coherence times enhancement in vanadium (iv)-based potential molecular qubits: the key role of the vanadyl moiety, *J. Am. Chem. Soc*., 2016, **138**, 11234–11244; (i) M. Atzori, L. Tesi, E. Morra, M. Chiesa, L. Sorace and R. Sessoli, Room-temperature quantum coherence and rabi oscillations in vanadyl phthalocyanine: toward multifunctional molecular spin qubits, *J. Am. Chem. Soc*., 2016, **138**, 2154–2157; (j) M. Urdampilleta, N. V. Nguyen, J. P. Cleuziou, S. Klyatskaya, M. Ruben and W. Wernsdorfer, Molecular quantum spintronics: Supramolecular spin valves based on single-molecule magnets and carbon nanotubes, *Int. J. Mol. Sci*., 2011, **12**, 6656-6667.

2 (a) N. Ishikawa, M. Sugita, T. Ishikawa, S. Koshihara and Y. Kaizu, Lanthanide double-decker complexes functioning as magnets at the single-molecular level, *J. Am. Chem. Soc*., 2003, **125**, 8694-8695; (b) J. D. Rinehart, M. Fang, W. J. Evans and J. R. Long, A N_2^{3-} radical-bridged terbium complex exhibiting magnetic hysteresis at 14 K, *J. Am. Chem. Soc*., 2011, **133**, 14236-14239; (c) J. D. Rinehart, M. Fang, W. J. Evans and J. R. Long, Strong exchange and magnetic blocking in N_2^{3-}-radical-bridged lanthanide complexes, *Nat. Chem*., 2011, **3**, 538-542; (d) D. N. Woodruff, R. E. P. Winpenny and R. A. Layfield, Lanthanide single-molecule magnets, *Chem. Rev.*, 2013, **113**, 5110-5148; (e) Y.-S. Ding, N. F. Chilton, R. E. P. Winpenny and Y.-Z. Zheng, On approaching the limit of molecular magnetic anisotropy: a near‐perfect pentagonal bipyramidal dysprosium (III) single‐molecule magnet, *Angew. Chem. Int. Ed.*, 2016, **55**, 16071-16074; (f) J. Liu, Y.-C. Chen, J.-L. Liu, V. Vieru, L. Ungur, J.-H. Jia, L. F. Chibotaru, Y. Lan, W. Wernsdorfer, S. Gao, X.-M. Chen and M.-L. Tong, A stable pentagonal bipyramidal Dy(III) single-ion magnet with a record magnetization reversal barrier over 1000 K, *J. Am. Chem. Soc*., 2016, **138**, 5441-5450; (g) C. A. P. Goodwin, F. Ortu, D. Reta, N. F. Chilton and D. P. Mills, Molecular magnetic hysteresis at 60 kelvin in dysprosocenium, *Nature*, 2017, **548**, 439-442; (h) F.-S. Guo, B. M. Day, Y.-C. Chen, M.-L. Tong, A. Mansikamäkki, and R. A. Layfield, A dysprosium metallocene single-molecule magnet functioning at the axial limit, *Angew. Chem., Int. Ed*., 2017, **56**, 11445-11449; (i) F.-S. Guo, B. M.

Day, Y.-C. Chen, M.-L. Tong, A. Mansikkamäki and R. A. Layfield, Magnetic hysteresis up to 80 kelvin in a dysprosium metallocene single-molecule magnet, *Science*, 2018, **362**, 1400-1403; (j) C. A. Gould, K. R. McClain, J. M. Yu, T. J. Groshens, F. Furche, B. G. Harvey and J. R. Long, Synthesis and magnetism of neutral, linear metallocene complexes of terbium (II) and dysprosium (II), *J. Am. Chem. Soc*., 2019, **141**, 12967-12973.

3 R. J. Glauber, Time-dependent statistics of the Ising model, *J. Math. Phys*., 1963, **4**, 294-307.

4 A. Caneschi, D. Gatteschi, N. Lalioti, C. Sangregorio, R. Sessoli, G. Venturi, A. Vindigni, A. Rettori, M. G. Pini and M. A. Novak, Cobalt (II)-nitronyl nitroxide chains as molecular magnetic nanowires, *Angew. Chem. Int. Ed*., 2001, **40**, 1760-1763.

5 (a) R. Clérac, H. Miyasaka, M. Yamashita, C. Coulon, Evidence for single-chain magnet behavior in a Mn^{III}-Ni^{II} chain designed with high spin magnetic units: a route to high temperature metastable magnets, *J. Am. Chem. Soc*., 2002, **124**, 12837–12844; (b) L. Bogani, A. Vindigni, R. Sessoli, D. Gatteschi, Single chain magnets: where to from here? *J. Mater. Chem*., 2008, **18**, 4750–4758; (c) H. Miyasaka, M. Julve, M. Yamashita, R. Clérac, Slow dynamics of the magnetization in one-dimensional coordination polymers: single-chain magnets, *Inorg. Chem*., 2009, **48**, 3420–3437; (d) C. Coulon, R. Clérac, W. Wernsdorfer, T. Colin and H. Miyasaka, Realization of a magnet using an antiferromagnetic phase of single-chain magnets, *Phys. Rev. Lett*., 2009, **102**, 167204; (e) H. L. Sun, Z. M. Wang, S. Gao, Strategies towards single-chain magnets, *Coord. Chem. Rev*., 2010, **254**, 1081–1100; (f) T. S. Venkatakrishnan, S. Sahoo, N. Bréfuel, C. Duhayon, C. Paulsen, A.-L. Barra, S. Ramasesha, J.-P. Sutter, Enhanced ion anisotropy by nonconventional coordination geometry: single-chain magnet behavior for a $[\{Fe^{II}L\}_2\{Nb^{IV}(CN)_8\}]$ helical chain compound designed with heptacoordinate Fe^{II}, *J. Am. Chem. Soc*., 2010, **132**, 6047–6056; (g) W. X. Zhang, R. Ishikawa, B. Breedlove, M. Yamashita, Single-chain magnets: beyond the Glauber model, *RSC Adv*., 2013, **3**, 3772–3798; (h) K. Bretosh, V. Béreau, C. Duhayon, C. Pichon, J.-P. Sutter. A ferromagnetic Ni(II)–Cr(III) single-chain magnet based on pentagonal bipyramidal building units, *Inorg. Chem. Front.* **2020**, DOI10.1039/C9QI01489F.

6 (a) N. Ishii, Y. Okamura, S. Chiba, T. Nogami and T. Ishida, Giant coercivity in a one-dimensional cobalt-radical coordination magnet, *J. Am. Chem. Soc*., 2008, **130**, 24−25; (b) Y. Okamura, T. Nogami and T. Ishida, The Hardest Magnet from a Coordination Polymer of Alternating Cobalt (II)–Radical Heterospins, *Chem. Lett*., 2009, **38**, 740−741; (c) M. G. F. Vaz, R. A. A. Cassaro, H. Akpinar, J. A. Schlueter, P. M. Lahti and M. A. Novak, A Cobalt Pyrenylnitronylnitroxide Single-Chain Magnet with High Coercivity and Record Blocking Temperature, *Chem. Eur. J*., 2014, **20**, 5460−5467; (d) R. A. A. Cassaro, S. G. Reis, T. S. Araujo, P. M. Lahti, M. A. Novak and M. G. F. Vaz, A single-chain magnet with a very high blocking temperature and a strong coercive field, *Inorg. Chem*., 2015, **54**, 9381−9383; (e) N. Ishii, T. Ishida and T. Nogami, Polymorphic Alternating HNN-Cobalt (II) Chains Both Behaving as Single-Chain Magnets (HNN= 4, 4, 5, 5-Tetramethylimidazolin-1-oxyl 3-Oxide), *Inorg. Chem*., 2006, **45**, 3837−3839; (f) Y. Okamura, N. Ishii, T. Nogami and T. Ishida, Hard Magnets after Freezing of Spin Dynamics of Soft Magnets in Cobalt (II)–Radical Chain Compounds, *Bull. Chem. Soc. Jpn*., 2010, **83**, 716−725; (g) X. X. Meng,

W. Shi and P. Cheng, Magnetism in one-dimensional metal–nitronyl nitroxide radical system, *Coord. Chem. Rev*., 2019, **378**, 134−150.

7 (a) L. Bogani, C. Sangregorio, R. Sessoli and D. Gatteschi, Molecular Engineering for Single-Chain-Magnet Behavior in a One-Dimensional Dysprosium–Nitronyl Nitroxide Compound, *Angew. Chem., Int. Ed*., 2005, **44**, 5817−5821; (b) K. Bernot, L. Bogani, A. Caneschi, D. Gatteschi and R. Sessoli, A family of rare-earth-based single chain magnets: playing with anisotropy, *J. Am. Chem. Soc.*, 2006, **128**, 7947-7956; (c) K. Benelli, J. Luzon, A. Caneschi, D. Gatteschi, R. Sessoli, L. Bogani, A. Vindigni, A. Rettori and M. G. Pini, Spin canting in a Dy-based single-chain magnet with dominant next-nearest-neighbor antiferromagnetic interactions, *Phys. Rev. B*, 2009, **79**, 134419; (d) R.-N. Liu, L.-C. Li, X.-L. Wang, P.-P. Yang, C. Wang, D.-Z. Liao and J.-P. Sutter, Smooth transition between SMM and SCM-type slow relaxing dynamics for a 1-D assemblage of {Dy(nitronyl nitroxide)$_2$} units, *Chem. Commun*., 2010, **46**, 2566-2568; (e) T. Han, W. Shi, Z. Niu, B. Na and P. Cheng, Magnetic blocking from exchange interactions: Slow relaxation of the magnetization and hysteresis loop observed in a dysprosium–nitronyl nitroxide chain compound with an antiferromagnetic ground state, *Chem.-Eur. J.*, 2013, **19**, 994−1001; (f) L. L. Li, S. Liu, H. Li, W. Shi and P. Cheng, Influence of external magnetic field and magnetic-site dilution on the magnetic dynamics of a one-dimensional Tb (III)–radical complex, *Chem. Commun*., 2015, **51**, 10933−10936.

8 (a) M. Zhu, P. Hu, Y. G. Li, X. F. Wang, L. C. Li, D. Z. Liao, V. M. L. Durga Prasad Goli, S. Ramasesha and J.-P. Sutter, Hetero-tri-spin [2p-3d-4f] Chain Compounds Based on Nitronyl Nitroxide Lanthanide Metallo-Ligands: Synthesis, Structure, and Magnetic Properties, *Chem. – Eur. J*., 2014, **20**, 13356-13365; (b) M. Zhu, X. L. Mei, Y. Ma, L.C. Li, D. Z. Liao and J.-P. Sutter, Nitronyl nitroxide–metal complexes as metallo-ligands for the construction of hetero-tri-spin (2p–3d–4f) chains, *Chem. Commun*., 2014, **50**, 1906-1908; (c) M. Zhu, L.-C. Li and J.-P. Sutter, 2p–3d–4f hetero-tri-spin molecule-based magnetic compounds, *Inorg. Chem. Front*., 2016, **3**, 994-1003.

9 S. G. McAdams, A.-M. Ariciu, A. K. Kostopoulos, J. P. S. Walsh, F. Tuna, Molecular single-ion magnets based on lanthanides and actinides: Design considerations and new advances in the context of quantum technologies, *Coord. Chem. Rev.*, 2017, **346**, 216-239.

10. M. L. Kahn, R. Ballou, P. Porcher, O. Kahn, J.-P. Sutter, Analytical Determination of the {Ln–Aminoxyl Radical} Exchange Interaction Taking into Account Both the Ligand-Field Effect and the Spin–Orbit Coupling of the Lanthanide Ion (Ln= Dy^{III} and Ho^{III}), *Chem. Eur. J.,* 2002, **8**, 525-531.

11 J. Xie, H. D. Li, M. Yang, J. Sun, L. C. Li and J.-P. Sutter, Improved single-chain-magnet behavior in a biradical-based nitronyl nitroxide-Cu-Dy chain, *Chem. Commun*., 2019, **55**, 3398-3401.

12 (a) F. Alonso, I. P. Beletskaya, M. Yus, Non-conventional methodologies for transition-metal catalysed carbon-carbon coupling: A critical overview. Part 2: The Suzuki reaction, *Tetrahedron*, 2008, 64, 3047-3101; (b) M. S. Davis, K. Morokuma and R. W. Kreilick, Free radicals with large negative spin densities, *J. Am. Chem. Soc.*, 1972, **94**, 5588-5592.

13 O. Kahn, Molecular Magnetism; VCH: Weinheim, 1993.

14 (a) G. M. Sheldrick, SHELXS-2014, Program for structure solution, Universität of Göttingen, Germany, 2014; (b) G. M. Sheldrick, SHELXL-2014, Program for structure refinement, Universität of Göttingen, Göttingen, Germany, 2014.

15 (a) D. Casanova, M. Llunell, P. Alemany and S. Alvarez, The Rich Stereochemistry of Eight-Vertex Polyhedra: A Continuous Shape Measures Study. *Chem. Eur. J*., 2005, **11**, 1479-1494; (b) M. Lluncll, D. Casanova, J. Circra, J. M. Bofill, P. Alcmany, S. Alvarez, M. Pinsky and D. Avnir, SHAPE, version 2.1; University of Barcelona: Barcelona, Spain, and Hebrew University of Jerusalem: Jerusalem, Israel, 2005.

16 J.-P. Sutter, M. L. Kahn, O. Kahn, Conclusive demonstration of the ferromagnetic nature of the interaction between holmium (III) and aminoxyl radicals, *Adv. Mater.* 1999, **11**, 863-865.

17 (a) J. J. Borrás-Almenar, J. M. Clemente-Juan, E. Coronado and B. S.Tsukerblat, High-nuclearity magnetic clusters: generalized spin Hamiltonian and its use for the calculation of the energy levels, bulk magnetic properties, and inelastic neutron scattering spectra. *Inorg. Chem*., 1999, **38**, 6081−6088; (b) J. J. Borrás-Almenar, J. M. Clemente-Juan, E. Coronado, B. S. Tsukerblat, MAGPACK A package to calculate the energy levels, bulk magnetic properties, and inelastic neutron scattering spectra of high nuclearity spin clusters. *J. Comput. Chem*. 2001, **22**, 985−991.

18 (a) M. L. Kahn, J.-P. Sutter, S. Golhen, P. Guionneau, L. Ouahab, O. Kahn and D. Chasseau, Systematic investigation of the nature of the coupling between a Ln (III) ion (Ln= Ce (III) to Dy (III)) and its aminoxyl radical ligands. structural and magnetic characteristics of a series of {Ln(organic radical)$_2$} compounds and the related {Ln(Nitrone)$_2$} derivatives, *J. Am. Chem. Soc*., 2000, **122**, 3413-3421; (b) K. Bernot, F. Pointillart, P. Rosa, M. Etienne, R. Sessoli and D. Gatteschi, Single molecule magnet behaviour in robust dysprosium–biradical complexes, *Chem. Commun*., 2010, **46**, 6458-6460; (c) C. Benelli, A. Caneschi, D. Gatteschi, L. Pardi, P. Rey, D. P. Shum and R. L. Carlin, Magnetic properties of lanthanide complexes with nitronyl nitroxides, *Inorg. Chem*., 1989, **28**, 272-275; (d) J.-P. Sutter, M. L. Kahn, S. Golhen, L. Ouahab and O. Kahn, Synthesis and Magnetic Behavior of Rare‐Earth Complexes with N, O-Chelating Nitronyl Nitroxide Triazole Ligands: Example of a [Gd^{III}{Organic Radical}$_2$] Compound with an S = 9/2 Ground State, *Chem. Eur. J*., 1998, **4**, 571-576; (e) J. Sun, Z. Sun, L. C. Li and J.-P. Sutter, Lanthanide–Nitronyl Nitroxide Chains Derived from Multidentate Nitronyl Nitroxides, *Inorg. Chem*., 2018, **57**, 7507-7511.

19 (a) D. Gatteschi, J. Laugier, P. Rey and C. Zanchini, Crystal and molecular structure and magnetic properties of the adducts of copper (II) hexafluoroacetylacetonate with the nitroxide ligand 2-phenyl-4, 4, 5, 5-tetramethylimidazoline-1-oxyl 3-oxide, *Inorg. Chem*., 1987, **26**, 938-943; (b) D. Luneau, P. Rey, J. Laugier, P. Fries, A. Caneschi, D. Gatteschi and R. Sessoli, Nitrogen-bonded copper(II)-imino nitroxide complexes exhibiting large ferromagnetic interactions, *J. Am. Chem. Soc*., 1991, **113**, 1245-1251; (c) A. Caneschi, D. Gatteschi, J. Laugier and P. Rey, Ferromagnetic alternating spin chains, *J. Am. Chem. Soc*., 1987, **109**, 2191-2192; (d) A. Caneschi, D. Gatteschi, A. Grand, J. Laugier, L. Pardi, P. Rey, Moderate ferromagnetic exchange between copper(II) and a nitronyl nitroxide in a square-pyramidal adduct. MO interpretation of the mechanism of exchange in copper (II)-nitroxide complexes, *Inorg. Chem*., 1988, **27**, 1031-1035; (e) B. Yao, Z. Guo, X. Zhang,

Y. Ma, Z. Yang, Q. Wang, L. C. Li and P. Cheng, A New Nitronyl Nitroxide Radical as Building Blocks for a Rare S= 13/2 High Spin Ground State 2p-3d Complex and a 2p-3d-4f Chain, *Cryst. Growth Des*., 2017, **17**, 95-99; (f) J. Sun, L. Xi, J. Xie, K. Wang, L. C. Li and J.-P. Sutter, A loop chain and a three-dimensional network assembled from a multi-dentate nitronyl nitroxide radical and $M(hfac)_2$ (M= Co^{II}, Cu^{II}), *Dalton Trans*., 2018, **47***,* 14630-14635.

20 (a) D. Shiomi, M. Tamura, H. Sawa, R. Kato and M. Kinoshita, Magnetic properties of an organic biradical, m-BNN: m-phenylene bis (α-nitronyl nitroxide), *J. Phys. Soc. Jpn*., 1993, **62**, 289-300; (b) L. Catala, J. L. Moigne, N. Kyritsakas, P. Rey, J. J. Novoa and P. Turek, Towards a Better Understanding of the Magnetic Interactions within m-Phenylene α-Nitronyl Imino Nitroxide Base Biradicals, *Chem. - Eur. J*., 2001, **7**, 2466−2480.

21 C. Benelli, A. Caneschi, D. Gatteschi, L. Pardi and P. Rey, Linear-Chain Gadolinium(III) Nitronyl Nitroxide Complexes with Dominant Next-Nearest-Neighbor Magnetic Interactions, *Inorg. Chem*., 1990, **29**, 4223−4228.

22 L. Xi, H. D. Li, J. Sun, Y. Ma, J. K. Tang, L.C. Li, Designing Multicoordinating Nitronyl Nitroxide Radical Towards Multinuclear Lanthanide Aggregates, *Inorg. Chem*., 2020, **59**, 443−451.

23 Coulon C, Miyasaka H, Clérac R, Single-Chain Magnets: Theoretical Approach and Experimental Systems, *Struct. Bond*., 2006, 122: 163-206.

24 (a) C. Dekker, A. F. M. Arts, H. W. de Wijn, A. J. van Duyneveldt and J. A. Mydosh, Activated dynamics in a two-dimensional Ising spin glass: $Rb_2Cu_{1-x}Co_xF_4$, *Phys. Rev. B*, 1989, **40**, 11243; (b) S. M. J. Aubin, Z. Sun, L. Pardi, J. Krzystek, K. Folting, L. C. Brunel, A. L. Rheingold, G. Christou, D. N. Hendrickson, Reduced anionic Mn_{12} molecules with half-integer ground states as single-molecule magnets, *Inorg. Chem*., 1999, **38**, 5329-5340.

Supporting Information

Contents

Table S1. Selected bond lengths [Å] and angles [°] for **1**.

Bond distances			
Gd(1)-O(3)	2.393(5)	Cu(2)-O(9)#1	1.927(6)
Gd(1)-O(2)	2.386(5)	Cu(2)-O(1)	2.386(6)
Gd(1)-O(13)	2.355(6)	Cu(2)-O(1)#1	2.386(6)
Gd(1)-O(18)	2.379(5)	Cu(2)-O(10)#1	1.934(6)
Gd(1)-O(15)	2.318(5)	Cu(2)-O(10)	1.934(6)
Gd(1)-O(17)	2.320(6)	Cu(3)-O(12)	1.927(5)
Gd(1)-O(16)	2.385(5)	Cu(3)-O(11)	1.936(6)
Gd(1)-O(14)	2.381(6)	Cu(3)-O(4)	2.611(6)
Cu(1)-O(8)	1.936(6)	Cu(3)-O(4)#1	2.611(6)
Cu(1)-O(5)	1.981(7)	O(3)-N(4)	1.293(8)
Cu(1)-N(1)	2.033(7)	O(2)-N(3)	1.302(8)
Cu(1)-O(7)	2.136(6)	N(5)-O(4)	1.271(8)
Cu(1)-O(6)	1.930(6)	N(2)-O(1)	1.275(8)
Cu(2)-O(9)	1.927(5)		
Angles			
O(2)-Gd(1)-O(3)	82.42(18)	O(6)-Cu(1)-O(8)	173.8(3)
O(13)-Gd(1)-O(3)	71.38(17)	O(6)-Cu(1)-O(5)	90.7(3)
O(13)-Gd(1)-O(2)	115.51(18)	O(6)-Cu(1)-N(1)	93.3(3)
O(13)-Gd(1)-O(18)	139.54(18)	O(6)-Cu(1)-O(7)	87.4(3)
O(13)-Gd(1)-O(16)	73.1(2)	O(9)#1-Cu(2)-O(9)	180
O(13)-Gd(1)-O(14)	72.3(2)	O(9)#1-Cu(2)-O(1)#1	93.2(2)
O(18)-Gd(1)-O(3)	70.70(17)	O(9)#1-Cu(2)-O(1)	86.8(2)
O(18)-Gd(1)-O(2)	72.57(18)	O(9)-Cu(2)-O(1)	93.2(2)
O(18)-Gd(1)-O(16)	130.95(18)	O(9)-Cu(2)-O(1)#1	86.8(2)
O(18)-Gd(1)-O(14)	140.5(2)	O(9)-Cu(2)-O(10)	87.6(2)
O(15)-Gd(1)-O(3)	83.7(2)	O(9)#1-Cu(2)-O(10)#1	87.6(2)
O(15)-Gd(1)-O(2)	146.57(19)	O(9)-Cu(2)-O(10)#1	92.4(2)
O(15)-Gd(1)-O(13)	88.3(2)	O(9)#1-Cu(2)-O(10)	92.4(2)
O(15)-Gd(1)-O(18)	74.15(18)	O(1)#1-Cu(2)-O(1)	180
O(15)-Gd(1)-O(17)	88.8(2)	O(10)-Cu(2)-O(1)	98.3(3)
O(15)-Gd(1)-O(16)	71.8(2)	O(10)#1-Cu(2)-O(1)#1	98.3(3)
O(15)-Gd(1)-O(14)	141.4(2)	O(10)#1-Cu(2)-O(1)	81.7(3)
O(17)-Gd(1)-O(3)	142.73(19)	O(10)-Cu(2)-O(1)#1	81.7(3)
O(17)-Gd(1)-O(2)	84.1(2)	O(10)#1-Cu(2)-O(10)	180
O(17)-Gd(1)-O(13)	145.0(2)	O(12)-Cu(3)-O(11)#2	86.8(2)
O(17)-Gd(1)-O(18)	72.13(19)	O(11)-Cu(3)-O(4)	78.8(2)
O(17)-Gd(1)-O(16)	72.9(2)	O(11)#2-Cu(3)-O(4)	101.2(2)
O(17)-Gd(1)-O(14)	89.0(2)	O(11)-Cu(3)-O(11)#2	180
O(16)-Gd(1)-O(3)	137.0(2)	O(12)#2-Cu(3)-O(4)	97.4(2)
O(16)-Gd(1)-O(2)	135.5(2)	O(12)-Cu(3)-O(4)	82.6(2)
O(14)-Gd(1)-O(3)	118.80(19)	O(12)#2-Cu(3)-O(12)	180
O(14)-Gd(1)-O(2)	71.3(2)	O(12)-Cu(3)-O(11)	93.2(2)
O(14)-Gd(1)-O(16)	70.7(2)	O(12)#2-Cu(3)-O(11)#2	93.2(2)
O(8)-Cu(1)-O(5)	85.3(3)	O(12)#2-Cu(3)-O(11)	86.8(2)
O(8)-Cu(1)-N(1)	92.7(3)	N(4)-O(3)-Gd(1)	139.2(4)
O(8)-Cu(1)-O(7)	89.3(3)	N(3)-O(2)-Gd(1)	136.8(5)
O(5)-Cu(1)-N(1)	143.7(3)	N(2)-O(1)-Cu(2)	149.2(6)
O(5)-Cu(1)-O(7)	107.6(3)	N(5)-O(4)-Cu(3)	144.3(5)
N(1)-Cu(1)-O(7)	108.6(3)		

#1 -x,-y+2,-z+1 #2 -x+1,-y+2,-z+1

Table S2. Selected bond lengths [Å] and angles [°] for **2**.

Bond distances			
Tb(1)-O(3)	2.391(6)	Cu(2)-O(10)	1.923(8)
Tb(1)-O(2)	2.383(6)	Cu(2)-O(10)#2	1.923(8)
Tb(1)-O(15)	2.312(6)	Cu(2)-O(1)#2	2.383(7)
Tb(1)-O(18)	2.384(6)	Cu(2)-O(1)	2.383(7)
Tb(1)-O(13)	2.365(7)	Cu(1)-O(6)	1.932(7)
Tb(1)-O(16)	2.379(6)	Cu(1)-O(8)	1.932(7)
Tb(1)-O(17)	2.328(7)	Cu(1)-O(7)	2.143(8)
Tb(1)-O(14)	2.384(7)	Cu(1)-O(5)	1.977(8)
Cu(3)-O(12)	1.922(6)	Cu(1)-N(1)	2.031(8)
Cu(3)-O(11)#1	1.941(6)	O(3)-N(4)	1.291(9)
Cu(3)-O(11)	1.941(6)	O(2)-N(3)	1.296(9)
Cu(3)-O(4)	2.610(7)	O(4)-N(5)	1.258(10)
Cu(2)-O(9)#2	1.927(6)	O(1)-N(2)	1.246(10)
Cu(2)-O(9)	1.927(6)		
Angles			
O(2)-Tb(1)-O(3)	81.8(2)	O(12)#1-Cu(3)-O(4)	97.0(3)
O(2)-Tb(1)-O(18)	72.4(2)	O(11)#1-Cu(3)-O(11)	180
O(2)-Tb(1)-O(14)	71.3(2)	O(11)#1-Cu(3)-O(4)	79.3(2)
O(15)-Tb(1)-O(3)	83.9(2)	O(11)-Cu(3)-O(4)	100.7(2)
O(15)-Tb(1)-O(2)	146.5(2)	O(9)#2-Cu(2)-O(9)	180
O(15)-Tb(1)-O(18)	74.3(2)	O(9)#2-Cu(2)-O(1)	93.8(3)
O(15)-Tb(1)-O(13)	88.0(3)	O(9)-Cu(2)-O(1)	86.2(3)
O(15)-Tb(1)-O(16)	71.5(2)	O(9)#2-Cu(2)-O(1)#2	86.2(3)
O(15)-Tb(1)-O(17)	88.8(3)	O(9)-Cu(2)-O(1)#2	93.8(3)
O(15)-Tb(1)-O(14)	141.5(3)	O(10)#2-Cu(2)-O(9)#2	92.9(3)
O(18)-Tb(1)-O(3)	71.1(2)	O(10)-Cu(2)-O(9)#2	87.1(3)
O(18)-Tb(1)-O(14)	140.1(3)	O(10)-Cu(2)-O(9)	92.9(3)
O(13)-Tb(1)-O(3)	71.1(2)	O(10)#2-Cu(2)-O(9)	87.1(3)
O(13)-Tb(1)-O(2)	115.3(2)	O(10)-Cu(2)-O(10)#2	180.0(5)
O(13)-Tb(1)-O(18)	139.6(2)	O(10)#2-Cu(2)-O(1)#2	97.8(4)
O(13)-Tb(1)-O(16)	72.9(3)	O(10)-Cu(2)-O(1)	97.8(4)
O(13)-Tb(1)-O(14)	72.8(3)	O(10)-Cu(2)-O(1)#2	82.2(4)
O(16)-Tb(1)-O(3)	136.7(3)	O(10)#2-Cu(2)-O(1)	82.2(4)
O(16)-Tb(1)-O(2)	136.3(2)	O(1)-Cu(2)-O(1)#2	180
O(16)-Tb(1)-O(18)	130.8(2)	O(6)-Cu(1)-O(8)	173.9(3)
O(16)-Tb(1)-O(14)	71.0(3)	O(6)-Cu(1)-O(7)	87.1(3)
O(17)-Tb(1)-O(3)	143.3(2)	O(6)-Cu(1)-O(5)	90.5(3)
O(17)-Tb(1)-O(2)	84.9(3)	O(6)-Cu(1)-N(1)	93.5(3)
O(17)-Tb(1)-O(18)	72.3(2)	O(8)-Cu(1)-O(7)	89.6(3)
O(17)-Tb(1)-O(13)	144.6(2)	O(8)-Cu(1)-O(5)	85.5(3)
O(17)-Tb(1)-O(16)	72.7(3)	O(8)-Cu(1)-N(1)	92.5(3)
O(17)-Tb(1)-O(14)	88.5(2)	O(5)-Cu(1)-O(7)	107.3(3)
O(14)-Tb(1)-O(3)	118.8(2)	O(5)-Cu(1)-N(1)	143.7(3)
O(12)-Cu(3)-O(12)#1	180	N(1)-Cu(1)-O(7)	108.9(3)
O(12)#1-Cu(3)-O(11)	92.8(3)	N(4)-O(3)-Tb(1)	139.3(5)
O(12)#1-Cu(3)-O(11)#1	87.2(3)	N(3)-O(2)-Tb(1)	137.9(6)
O(12)-Cu(3)-O(11)	87.2(3)	N(5)-O(4)-Cu(3)	145.0(6)
O(12)-Cu(3)-O(11)#1	92.8(3)	N(2)-O(1)-Cu(2)	150.1(8)
O(12)-Cu(3)-O(4)	83.0(3)		

#1 -x,-y,-z #2 -x+1,-y,-z

Table S3. Selected bond lengths [Å] and angles [°] for **3**.

Bond distances			
Ho(1)-O(3)	2.362(4)	Cu(2)-O(10)	1.934(5)
Ho(1)-O(2)	2.359(4)	Cu(2)-O(10)#2	1.934(5)
Ho(1)-O(15)	2.284(4)	Cu(2)-O(1)	2.372(4)
Ho(1)-O(16)	2.366(4)	Cu(2)-O(1)#2	2.372(4)
Ho(1)-O(18)	2.363(4)	Cu(1)-O(7)	2.140(4)
Ho(1)-O(14)	2.341(4)	Cu(1)-O(6)	1.945(4)
Ho(1)-O(13)	2.333(4)	Cu(1)-O(8)	1.937(4)
Ho(1)-O(17)	2.296(4)	Cu(1)-O(5)	1.986(5)
Cu(3)-O(12)	1.940(4)	Cu(1)-N(1)	2.025(5)
Cu(3)-O(11)	1.930(4)	O(3)-N(4)	1.293(6)
Cu(3)-O(4)#1	2.583(4)	O(2)-N(3)	1.298(6)
Cu(3)-O(4)	2.583(4)	O(4)-N(5)	1.278(7)
Cu(2)-O(9)#2	1.940(4)	O(1)-N(2)	1.264(7)
Cu(2)-O(9)	1.940(4)		
Angles			
O(3)-Ho(1)-O(16)	137.62(15)	O(11)-Cu(3)-O(12)	92.98(17)
O(3)-Ho(1)-O(18)	69.80(13)	O(11)#1-Cu(3)-O(12)	87.02(17)
O(2)-Ho(1)-O(3)	82.45(13)	O(11)-Cu(3)-O(11)#1	180
O(2)-Ho(1)-O(16)	135.01(15)	O(11)-Cu(3)-O(4)#1	97.47(16)
O(2)-Ho(1)-O(18)	72.26(13)	O(11)#1-Cu(3)-O(4)	97.47(16)
O(15)-Ho(1)-O(3)	83.75(14)	O(11)-Cu(3)-O(4)	82.53(16)
O(15)-Ho(1)-O(2)	146.00(14)	O(4)#1-Cu(3)-O(4)	180
O(15)-Ho(1)-O(16)	72.43(15)	O(9)-Cu(2)-O(9)#2	180
O(15)-Ho(1)-O(18)	73.83(13)	O(9)#2-Cu(2)-O(1)#2	87.94(17)
O(15)-Ho(1)-O(14)	142.06(15)	O(9)#2-Cu(2)-O(1)	92.06(17)
O(15)-Ho(1)-O(13)	88.23(15)	O(9)-Cu(2)-O(1)	87.94(17)
O(15)-Ho(1)-O(17)	88.50(16)	O(10)#2-Cu(2)-O(9)#2	92.60(19)
O(18)-Ho(1)-O(16)	131.59(13)	O(10)-Cu(2)-O(9)	92.60(19)
O(14)-Ho(1)-O(3)	119.24(14)	O(10)-Cu(2)-O(9)#2	87.40(19)
O(14)-Ho(1)-O(2)	70.97(16)	O(10)-Cu(2)-O(10)#2	180
O(14)-Ho(1)-O(16)	70.58(15)	O(10)#2-Cu(2)-O(1)	81.5(2)
O(14)-Ho(1)-O(18)	140.13(16)	O(10)-Cu(2)-O(1)	98.5(2)
O(13)-Ho(1)-O(3)	71.61(13)	O(10)#2-Cu(2)-O(1)#2	98.5(2)
O(13)-Ho(1)-O(2)	116.25(13)	O(1)-Cu(2)-O(1)#2	180
O(13)-Ho(1)-O(16)	73.08(15)	O(6)-Cu(1)-O(7)	87.17(19)
O(13)-Ho(1)-O(18)	138.78(14)	O(6)-Cu(1)-O(5)	90.8(2)
O(13)-Ho(1)-O(14)	73.29(17)	O(6)-Cu(1)-N(1)	92.79(19)
O(17)-Ho(1)-O(3)	142.84(14)	O(8)-Cu(1)-O(7)	89.74(18)
O(17)-Ho(1)-O(2)	84.08(15)	O(8)-Cu(1)-O(6)	174.27(19)
O(17)-Ho(1)-O(16)	72.31(17)	O(8)-Cu(1)-O(5)	85.5(2)
O(17)-Ho(1)-O(18)	73.13(14)	O(8)-Cu(1)-N(1)	92.75(19)
O(17)-Ho(1)-O(14)	88.24(16)	O(5)-Cu(1)-O(7)	107.0(2)
O(17)-Ho(1)-O(13)	144.57(15)	O(5)-Cu(1)-N(1)	144.9(2)
O(12)#1-Cu(3)-O(12)	180	N(1)-Cu(1)-O(7)	108.0(2)
O(12)-Cu(3)-O(4)	78.50(16)	N(4)-O(3)-Ho(1)	138.7(3)
O(12)#1-Cu(3)-O(4)	101.50(16)	N(3)-O(2)-Ho(1)	136.6(4)
O(12)#1-Cu(3)-O(4)#1	78.50(16)	N(5)-O(4)-Cu(3)	143.8(4)
O(11)-Cu(3)-O(12)#1	87.02(17)	N(2)-O(1)-Cu(2)	147.3(5)
O(11)#1-Cu(3)-O(12)#1	92.98(17)		

#1 -x,-y+1,-z #2 -x+1,-y+1,-z

Table S4. SHAPE analysis for the Ln coordination spheres for **1**-**3**.

Compound	SAPR-8	TDD-8	JBTPR-8	BTPR-8	JSD-8
1 Gd	2.090	1.884	1.540	0.771	3.718
2 Tb	2.059	1.792	1.526	0.754	3.689
3 Ho	2.134	1.918	1.474	0.744	3.712

SAPR-8: Square antiprism; TDD-8: Triangular dodecahedron; JBTPR-8: Biaugmented trigonal prism J50; BTPR-8: Biaugmented trigonal prism; JSD-8: Snub diphenoid J84.

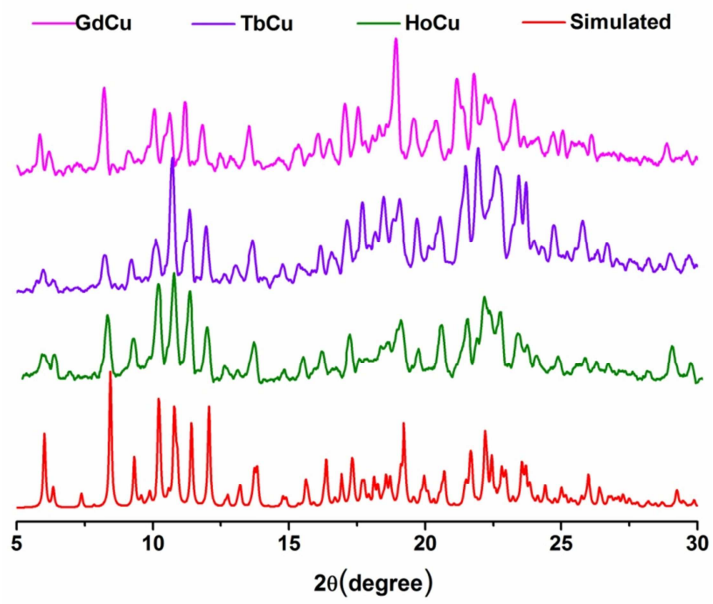

Fig. S1 Powder X-ray diffraction patterns of complexes **1**-**3**.

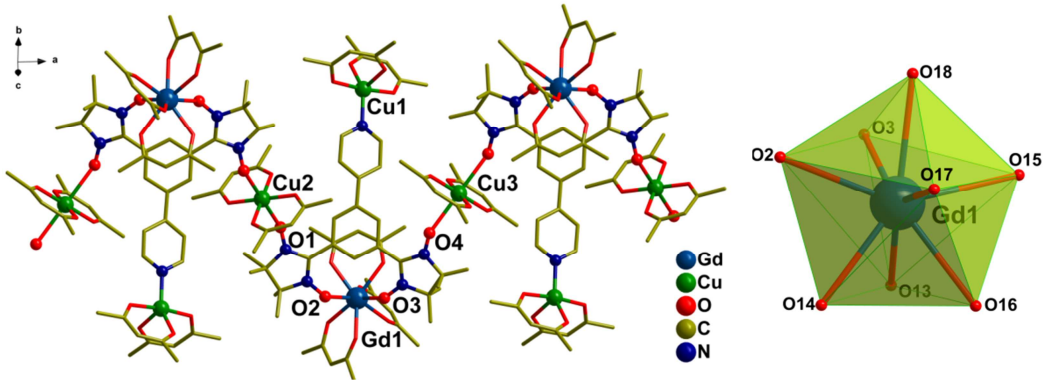

Fig. S2 One-dimensional structure of **1** and local coordination geometry of Gd(III) ion (Fluorine and Hydrogen atoms are omitted for the sake of clarity).

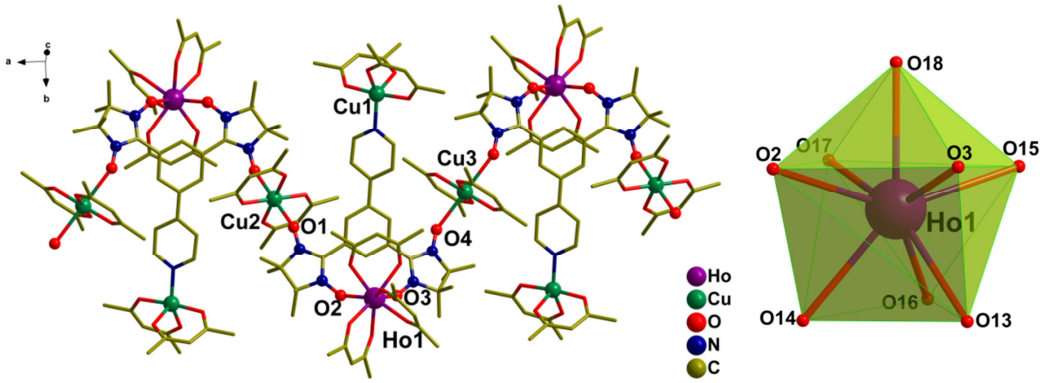

Fig. S3 One-dimensional structure of **3** and local coordination geometry of Ho(III) ion (Fluorine and Hydrogen atoms are omitted for the sake of clarity).

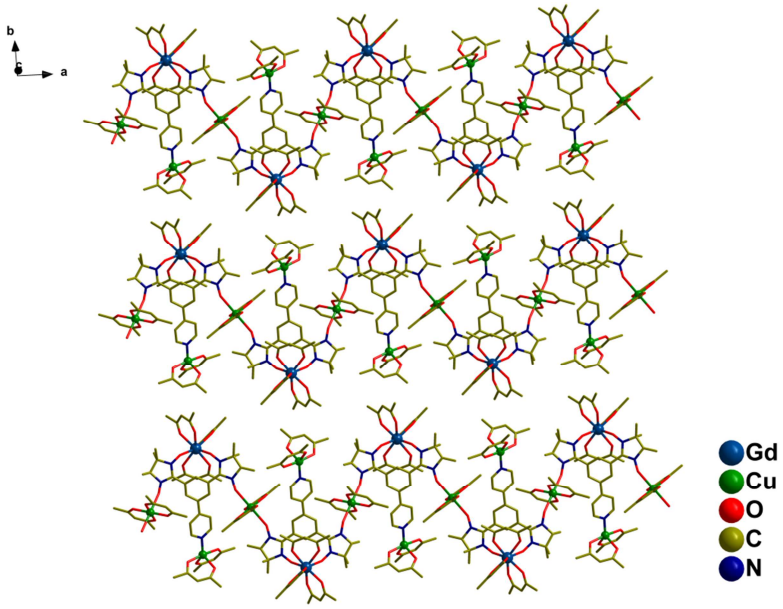

Fig. S4 Packing arrangement of the chains in **1** (H and F atoms are omitted for clarity).

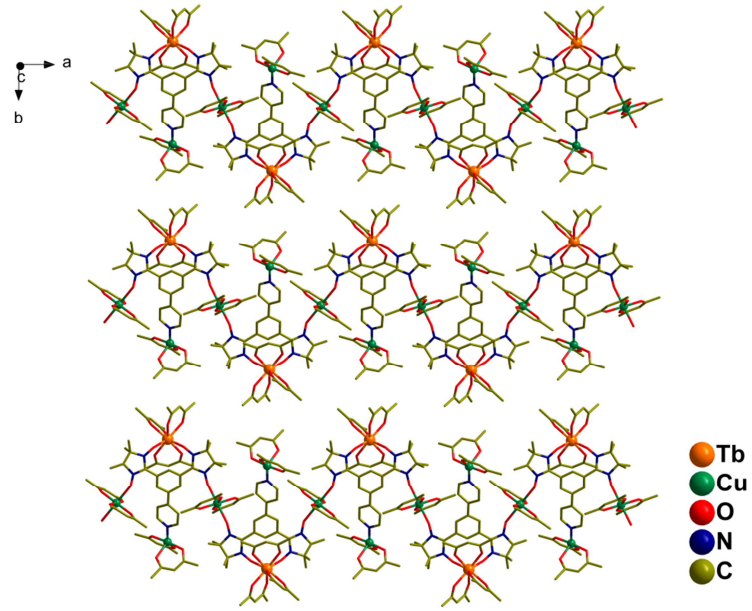

Fig. S5 Packing arrangement of the chains in **2** (H and F atoms are omitted for clarity).

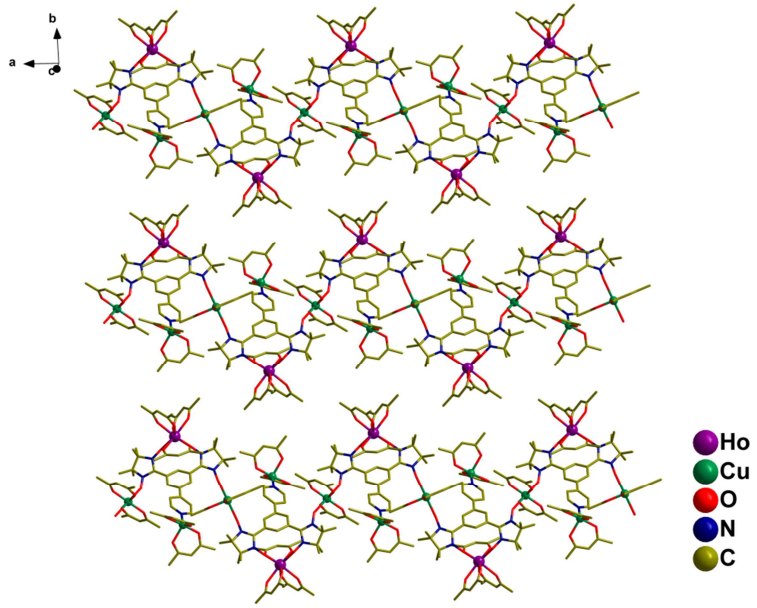

Fig. S6 Packing arrangement of the chains in **3** (H and F atoms are omitted for clarity).

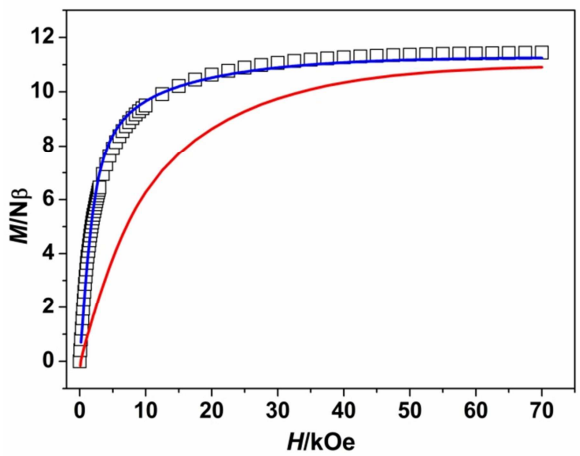

Fig. S7 Plot of magnetization *vs* field for **1** at 2 K. The blue line is the calculated curve using Magpack program, and the red line shows the theoretical behavior for one S =7/2 and four S =1/2 non-coupled spins (see the text).

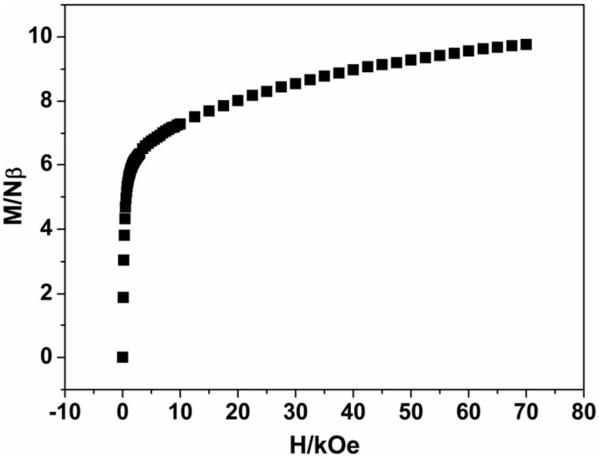

Fig. S8 Plot of magnetization *vs* field for **2** at 2 K.

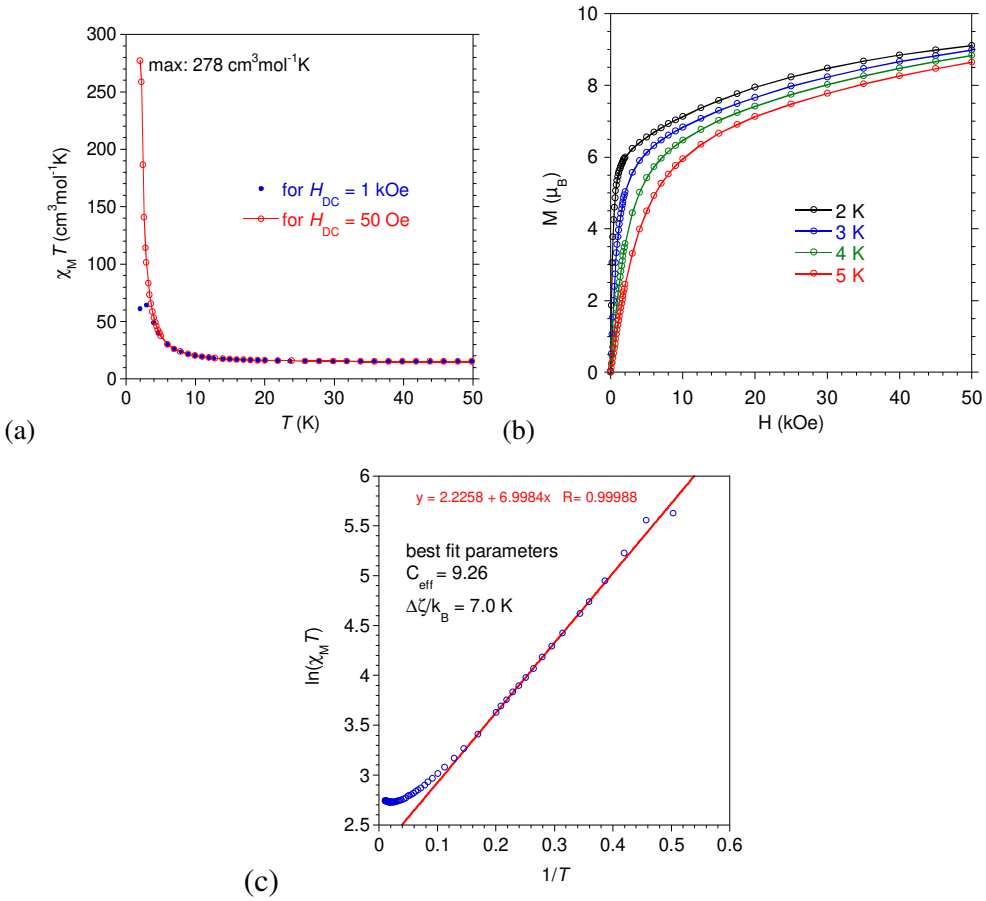

Fig. S9 Compound **3**: (a) $\chi_M T$ = f(T) for susceptibility data obtained in a field of 50 Oe (in red) and 1 kOe (in blue); (b) magnetization *vs* field at 2 K, 3 K, 4 K and 5 K; (c) $\ln(\chi_M T) = f(1/T)$ and best fit of the linear section between 2.5 and 5 K.

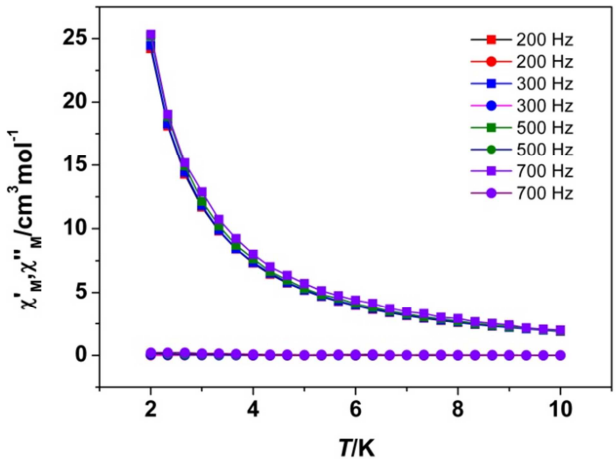

Fig. S10 Temperature dependence of in phase (χ') and out of phase (χ'') of **1** in 0 Oe dc field with an oscillation of 3 Oe.

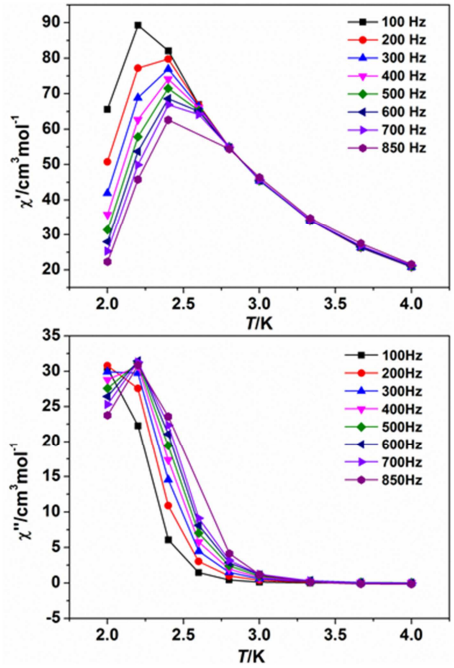

Fig. S11 Temperature-dependent ac signals under a zero dc field for compound **2**.

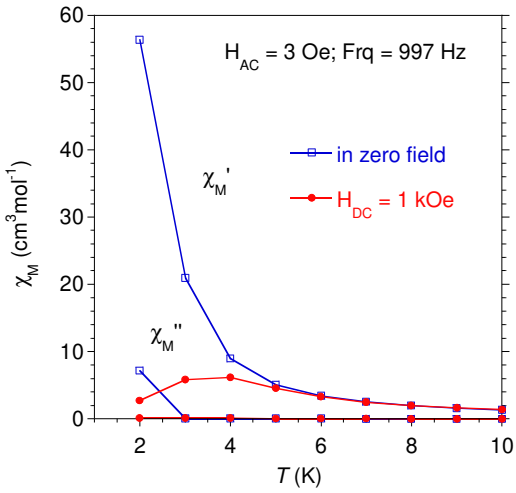

Fig. S12. Compound **3**: χ_M' and $\chi_M'' = f(T)$ in zero and 1 kOe dc field between 2-10 K.